Decay of Nanostructures

F. Hausser* and A. Voigt**

Crystal Growth Group, Research Center caesar, Ludwig-Erhard-Allee 2, 53175 Bonn, Germany,
*hausser@caesar.de, **voigt@caesar.de

ABSTRACT

The thermal relaxation of isolated (single layer) homoepitaxial islands and craters and of isolated nanomounds is simulated using a 2+1 dimensional step flow model. Numerical simulations based on adaptive finite elements are used to study the decay rates of these structures in the diffusion limited and the attachment-detachment limited regime under the influence of anisotropic effects.

Keywords: homoepitaxy, Ehrlich-Schwoebel barrier, thermal relaxation, anisotropy, adaptive finite elements

1 INTRODUCTION

Since many nanometer structures are easy to relax at high temperatures, a quantitative understanding of the thermal relaxation of nanostructures is important for the development of nanometer fabrication. In [1], [2] the decay of silicon hillocks, craters and mounds on a Si(111) surfaces is measured by scanning tunneling microscopy. These experiments clearly show a discrete single layer mode of the decay as well as several scaling exponents for the decay rates. Theoretical studies of such a decay were until now restricted to either purely periodic or rotational symmetric settings [3], [4]. We will extend this work to full 2+1 dimensional situations and simulate decay rates in an anisotropic setting.

The goal of our work is to establish an efficient and accurate framework for simulating decay processes. Most approaches to the simulation of nanostructure decay are based on phenomenological models treating the crystal surface as a continuous height function and ignore the discrete nature of surface steps. Our approach – based on a step-flow model – allows a more detailed description of the surface evolution and also the direct incorporation of important microscopic effects such as the Ehrlich Schwoebel barrier, step edge diffusion, step-step interactions and line tension. Still the model allows – much more then purely microscopic models – efficient simulations over a long time scale, where thermal relaxation takes place.

An adaptive finite element framework for these class of problems has been developed by the authors in [5], [6]. The step flow model consists of an adatom (adsorbed atom) diffusion equation on terraces of different height; boundary conditions on terrace boundaries including anisotropic line tension and the kinetic asymmetry in the adatom attachment and detachment; and the normal velocity law for the motion of such boundaries determined by a two-sided flux, together with the (possibly anisotropic) diffusion of edge-adatoms along the step-edges.

After describing the model and the numerical algorithm, the method is shown to be accurate and efficient for the numerical simulation of attachment/detachment-limited (AL) and diffusion-limited (DL) cases. The influence of different attachment rates on the decay of single-layer islands (or craters) is investigated. As a numerical benchmark, we compare our fully 2+1 dimensional simulation of the decay of a concentric rotational symmetric crystalline cone with an ODE simulation also recovering the well known $t^{1/4}$ decay law, see [3]. The simulation of the decay of a nanomound with anisotropic line tension agrees qualitatively with experiments shown in [2].

2 STEP FLOW MODEL

We denote by $\Omega \subset \mathbb{R}^2$ the projected domain of the film surface and assume that Ω is independent of time t. Moreover $\Omega_0 = \Omega_0(t) \subset \Omega$ denotes the projected domain of the substrate or the exposed film surface with the smallest layer thickness and $\Omega_i = \Omega_i(t) \subset \Omega$, $i = 1, \ldots, N$, the projected domain of the terrace of height i at time t, respectively. Thus, $N+1$ is the total number of layers that are exposed on the film surface. The corresponding steps are denoted by $\Gamma_i(t) = \overline{\Omega_i(t)} \cap \overline{\Omega_{i-1}(t)}$, $i = 1, \ldots, N$. Denote by $\rho_i = \rho_i(x,t)$ the adatom density on terrace $\Omega_i(t)$ $(i = 0, \ldots N)$ at time t. The adatom diffusion on a terrace is described by the diffusion equation for the adatom density

$$\partial_t \rho_i - \nabla \cdot (D \nabla \rho_i) = F - \tau^{-1} \rho_i \qquad \text{in } \Omega_i(t), \tag{1}$$

where $D > 0$ is the surface diffusivity, $F \geq 0$ is the deposition flux rate, and $\tau^{-1} \geq 0$ is the desorption rate. Throughout the paper the unit of length will be the substrate lattice spacing a. Thus the adatom density ρ denotes the number of adatoms per adsorption site.

Now let j_i^+, j_i^- be the adatom flux at the boundary Γ_i from the upper and lower terrace, respectively, which are given by

$$j_i^+ := -D\nabla\rho_i \cdot \vec{n}_i - v_i\rho_i \tag{2}$$

$$j_i^- := D\nabla\rho_{i-1} \cdot \vec{n}_i + v_i\rho_{i-1}, \tag{3}$$

where $\vec{n}_i$ and v_i are the unit normal pointing from the upper to the lower terrace and the normal velocity of the step $\Gamma_i(t)$, respectively, with the convention that $v_i > 0$ if the movement of $\Gamma_i(t)$ is in the direction of $\vec{n}_i$.

Assuming the attachment/detachment limited case, the adatom density satisfies the following kinetic boundary conditions on the island boundary $\Gamma_i(t)$

$$j_i^+ = k_+(\rho_i - \rho_i^{eq}), \tag{4}$$

$$j_i^- = k_-(\rho_{i-1} - \rho_{i-1}^{eq}), \tag{5}$$

where ρ_i^{eq} is the equilibrium density at Γ_i. Here we assume that the steps are non permeable, i.e. there is no adatom diffusion across a step that bypasses attachment to the step. Permeability may be built into the model by adding a term being proportional to $\rho_i - \rho_{i-1}$ to the fluxes at the steps.

With this notation $0 < k_+ < k_-$ models the Ehrlich-Schwoebel effect. If $k_+, k_- \to \infty$, i.e. the diffusion limited case, Eqs. (4) and (5) pass into the thermodynamic boundary condition

$$\rho_i = \rho_{i-1} = \rho_i^{eq}.$$

The equilibrium adatom density ρ_i^{eq} is described by the Gibbs-Thomson-type relation

$$\rho_i^{eq} = \rho^* \exp\left(\frac{\mu}{k_B T}\right) \approx \rho^*(1 + \frac{\mu_i}{k_B T}), \tag{6}$$

where μ_i is the anisotropic chemical potential of the boundary Γ_i, being given as the first variation of the step free energy, and ρ^* is a positive constant denoting the thermodynamic equilibrium density at a straight non interacting step. If γ denotes the orientation dependent step free energy divided by $k_B T$, and

$$\tilde{\gamma}(\theta) = \gamma(\theta) + \gamma_{\theta\theta}(\theta),$$

with θ the angle of the outer normal with the x-axis, we obtain

$$\frac{\mu_i}{k_B T} = \tilde{\gamma}\kappa_i, \quad \text{i.e.,} \quad \rho_i^{eq} = \rho^*(1 + \tilde{\gamma}\kappa_i), \tag{7}$$

where κ_i is the curvature of the boundary $\Gamma_i(t)$. To model step-step interaction, a force term is added to the chemical potential μ_i (i.e. the normal derivative of a step interaction potential being part of the step free energy). Assuming, that the steps are interacting via elastic repulsion a nearest neighbor potential being inversely proportional to the average distance of neighboring steps as in [3] is used.

For the motion of the steps, we assume the following law for the normal velocity v_i of the island boundary $\Gamma_i(t)$

$$v_i = j_i^+ + j_i^- + \partial_s(\nu\partial_s(\tilde{\gamma}\kappa_i)), \tag{8}$$

where ν is a positive function denoting the (orientation dependent) mobility of the edge diffusion, and ∂_s denotes the tangential derivative along the steps. The last term in Eq. (8) represents step edge diffusion of edge-adatoms along the steps, whereas the first two terms ensure the adatom mass conservation.

In order to study the decay rates, small islands are placed on a large exposed film surface Ω_0. The boundary of Ω_0 is modeled as a fixed step. This leads to Robin type conditions for the adatom density at the domain boundary which ensures a realistic comparison with the experimental results.

For a circular, isolated monolayer island the radius decays approximately as $R(t) \approx t^{1/3}$ in the diffusion limited case and as $R(t) \approx t^{1/2}$ in the attachment/detachment limited case. This was already shown in rotational symmetric setting in [4] and follows from a quasi-stationary approximation of (1) with $F = \tau^{-1} = 0$. For $k = k_+ = k_-$ and $j_0^+ = k(\rho_0 - \rho^*)$, this yields

$$\dot{R} = -\frac{\rho^*\tilde{\gamma}k}{R}\frac{1/R}{(1/R + 1/R_0) + k/D\ln(R_0/R)}, \tag{9}$$

with $R_0 \gg R$ being the radius of Ω_0. In the attachment/detachment limited case ($k/D \to 0$) this leads to $\dot{R} \approx -R^{-1}$ and in the diffusion limited case ($k/D \to \infty$) to $\dot{R} \approx -R^{-2}$, implying the described decay rates.

3 DISCRETIZATION

We shortly review the weak formulation and finite element discretization as introduced in [5], [6]. In each time step: (i) we update the discrete step boundaries by solving a geometric partial differential equation based on the adatom densities and the discrete step boundaries from the previous time step; (ii) we solve the diffusion equation to update the adatom densities using the adatom densities from the previous time step and the computed discrete representation of the steps.

3.1 Boundary evolution

We describe the discretization without step-step interaction. The incorporation of the latter is straight forward by modifying the chemical potential as described above. Using the boundary conditions Eqs. (4) and (5) at $\Gamma_i(t)$ in the velocity formula Eq. (8) leads to the geometric PDE

$$v_i = \gamma_i + \beta\tilde{\gamma}\kappa_i + \partial_s(\nu\partial_s(\tilde{\gamma}\kappa_i)), \tag{10}$$

with $\gamma_i = k_+(\rho_i - \rho^*) + k_-(\rho_{i-1} - \rho^*)$ and $\beta = (k_+ + k_-)\rho^*$. This equation can be interpreted as an equation for anisotropic (one dimensional) "surface" diffusion with lower order terms. A variational formulation and discretization using parametric finite elements is obtained as follows. Introducing the position vector $\vec{x}_i$, the curvature vector $\kappa_i = \vec{\kappa}_i \cdot \vec{n}_i$, and the velocity vector $\vec{v}_i = v_i \vec{n}_i$, and using the geometric expression $\vec{\kappa}_i = -\partial_{ss}\vec{x}_i$, Eq. (10) becomes equivalent to the following system of equations for $\vec{\kappa}_i$, κ_i, v_i, and $\vec{v}_i$.

$$\vec{\kappa}_i = -\partial_{ss}(\vec{x}_i), \tag{11}$$

$$\kappa_i = \vec{\kappa}_i \cdot \vec{n}_i, \tag{12}$$

$$v_i = \gamma_i - \beta\tilde{\gamma}\kappa_i + \partial_s(\nu\partial_s(\tilde{\gamma}\kappa_i)), \tag{13}$$

$$\vec{v}_i = v_i \vec{n}_i. \tag{14}$$

Considering discrete time steps Δt, the boundary at time $t + \Delta t$ is represented in terms of the boundary at time t by updating the position vector $\vec{x}_i \leftarrow \vec{x}_i + \Delta t \vec{v}_i$. Plugging the updated position vector into Eq. (11) and multiplying Eqs. (11) - (14) with test functions ψ and $\vec{\psi}$ leads to the following weak formulation:

$$\int_{\Gamma_i} \vec{\kappa}_i\vec{\psi} - \Delta t \int_{\Gamma_i} \partial_s\vec{v}_i \cdot \partial_s\vec{\psi} = \int_{\Gamma_i} \partial_s\vec{x}_i \cdot \partial_s\vec{\psi},$$

$$\int_{\Gamma_i} \kappa_i\psi - \int_{\Gamma_i} \vec{\kappa}_i \cdot \vec{n}_i\psi = 0,$$

$$\int_{\Gamma_i} v_i\psi + \int_{\Gamma_i} \nu\partial_s(\tilde{\gamma}\kappa_i) \cdot \partial_s\psi + \int_{\Gamma_i} \beta\tilde{\gamma}\kappa_i\psi = \int_{\Gamma_i} \gamma_i\psi,$$

$$\int_{\Gamma_i} \vec{v}_i\vec{\psi} - \int_{\Gamma_i} v_i\vec{n}_i\vec{\psi} = 0.$$

The system is now discretized using parametric finite elements. Note that in the above formulation, the adatom densities ρ_i and ρ_{i-1} on the upper and lower terraces, respectively, are needed only for computing γ_i. Solving the resulting linear system on each boundary yields the new boundary. These new boundaries, together with their curvatures will enter in the next time-step for the adatom diffusion.

3.2 Adatom diffusion

We now shortly discribe the discretization of the adatom diffusion equation in the attachment limited case without step permeability. For the discretization of the diffusion limited case, a slightly different approach based on a penalty method is used, see Ref. [6]. Multiplying Eq. (1) by a test function ϕ and integration by parts leads to

$$\begin{aligned}\int_{\Omega_i} \partial_t\rho_i\phi + \int_{\Omega_i} D\nabla\rho_i \cdot \nabla\phi \\ + \int_{\Gamma_{i+1}} D\nabla\rho_i \cdot \vec{n}_{i+1}\phi - \int_{\Gamma_i} D\nabla\rho_i \cdot \vec{n}_i\phi \\ = \int_{\Omega_i} F\phi - \int_{\Omega_i} \tau^{-1}\rho_i\phi.\end{aligned}$$

For each i this equation is extended to the whole time-independent domain Ω by setting $\rho_i, D_i, F_i, \tau_i^{-1} = 0$ outside of Ω_i. Taking account of the distributional time-derivatives of ρ_i at the steps, denoted by $\dot{\rho}_i$, and using the boundary conditions Eqs. (4) and (5) we obtain

$$\begin{aligned}\int_\Omega \dot{\rho}_i\phi + \int_\Omega D_i\nabla\rho_i \cdot \nabla\phi \\ + \int_{\Gamma_{i+1}(t)} k_-(\rho_i - \rho^*(1 + \tilde{\gamma}\kappa_{i+1}))\phi \\ + \int_{\Gamma_i(t)} k_+(\rho_i - \rho^*(1 + \tilde{\gamma}\kappa_i))\phi \\ = \int_\Omega F_i\phi + \int_\Omega \tau_i^{-1}\rho_i\phi.\end{aligned} \tag{15}$$

Notice, that for the derivation of Eq. (15) the convective terms in Eqs. (4) and (5) are essential. Since Eq. (15) is solved for each ρ_i on the whole domain, there are two degrees of freedom at each boundaries $\Gamma_i(t)$, namely ρ_i and ρ_{i-1}. This way the discontinuity in the adatom density at the steps can be resolved. Eq. (15) is discretized using an implicit Euler discretization in time and linear finite elements in space. An adaptive strategy is used in order to refine the numerical mesh close to the step edges.

4 Numerical results

Simulating the decay of nanostructures requires large time-scales. For the algorithm to be efficient it is indispensable to use adaptivity in time. We chose the time step depending on the maximal velocity of the step boundaries. If not otherwise stated, the parameters are $D = 10^5$, $\tau^{-1} = 0$, $\gamma = 0.1$ and $\rho^* = 10^{-4}$.

4.1 Decay of single layer islands and craters

The decay of monolayer islands (or craters) with initial area 100π on a substrate of 600×600 is simulated. In the isotropic case, the initial island boundary is a circle and in the anisotopic case it is the Wulff shape of the anisotropy function $\gamma(\theta) = 0.1 + 0.01\cos(3\theta)$, see Fig. 1.

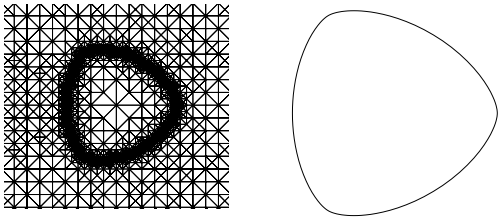

Figure 1: Adaptively refined two-dimensional mesh and 1d island boundary in the anisotropic case.

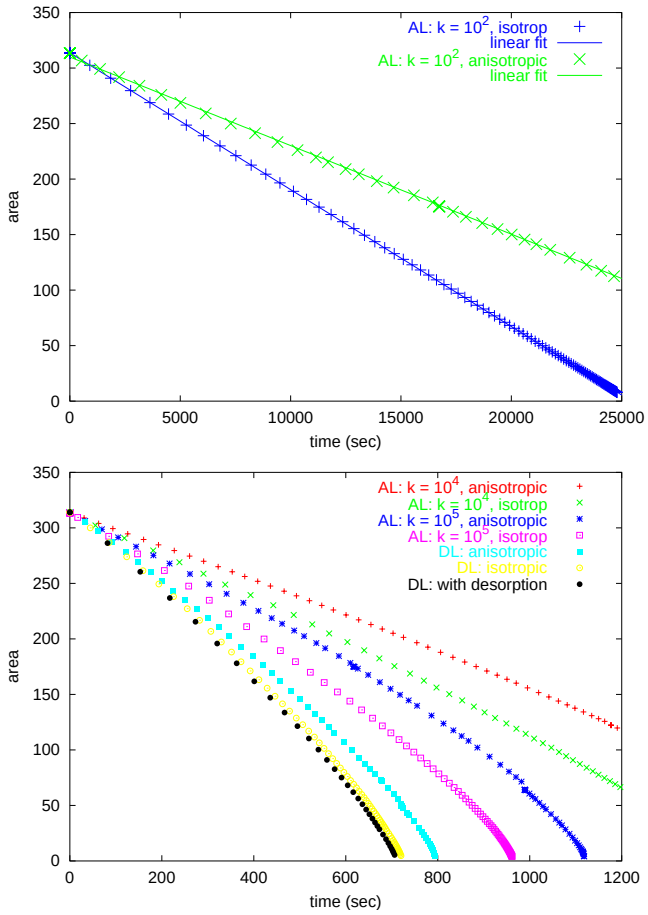

Figure 2: Decay of single layer island: linear decay for low attachment rate k (top), attachment limited decay with increasing k and diffusion limited decay

As shown in Fig. 2(top), the decay for a small attachment/detachment rate k ($k/D = 10^{-3}$) becomes linear. With increasing k, the decay curves approximate the diffusion limited case, see Fig. 2(bottom). Desorption has a very small effect on the decay rates (we used a desorption rate of $\tau^{-1} = 10^{-4}$). The anisotropy does not change the qualitativ picture of the decay rates but slows down the decay process.

4.2 Decay of isolated nanomounds

A comparison of a 2+1 dimensional simulation of the decay of a circular cone with 15 layers with the rotational symmetric ODE solution shows acurate quantitative agreement including a decay rate of $t^{1/4}$ of the top island radius as in [3] (not shown here). Here we present the simulation of the decay of an anisotropic mound with 12 atomic layers. The inital shape of the top terrace of the pyramid is nearly hexagonal, while the shape at the bottom is a rounded triangle and we use an anisotropy γ with hexagonal symmetry. Fig. 3 shows the discrete height profile of the mound during decay. As can be seen, the bottom layer becomes a rounded

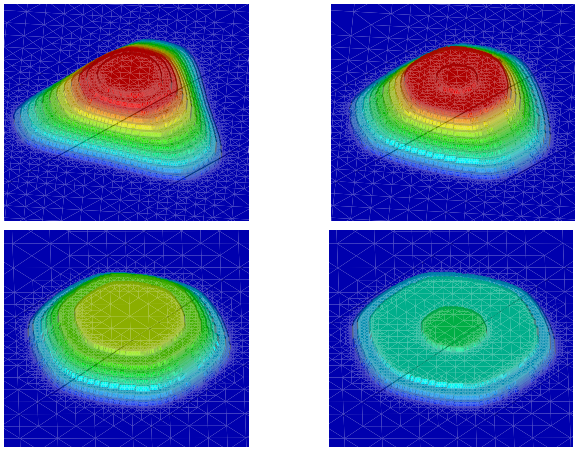

Figure 3: Anisotropic decay of a nanomound on a substrate of size 200×200 (in units of lattice constant). Discrete heights at time = 12, 65, 476, 1330 seconds.

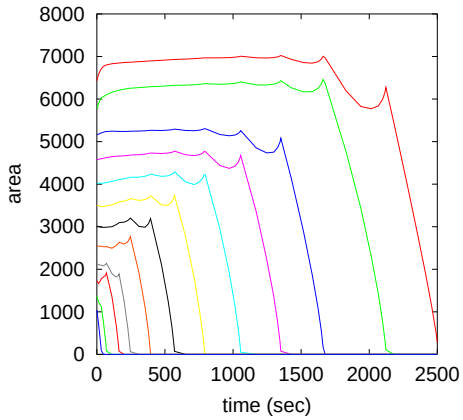

Figure 4: Layer by layer decay of the nanomounds with 12 atomic layers as in Fig. 3

hexagon. In Fig. 4 the layer by layer decay is shown. The setting is chosen similar to the experimental decay of Si mounds studied in [2] and shows qualitative agreement with their results.

REFERENCES

[1] A. Ichimiya, Y. Tanaka, and K. Ishiyama. *Phys. Rev. Lett.*, 76:4721–4724, 1996.

[2] A. Ichimiya, K. Hayashi, E.D Williams, T.L. Einstein, M. Uwaha, and K. Watanabe. *Phys. Rev. Lett.*, 84:3662–3665, 2000.

[3] N. Israeli and D. Kandel. *Phys. Rev. B*, 60(8):5946–5962, 1999.

[4] M. Uwaha and K. Watanabe. *J. Phys. Soc. Jpn.*, 69(2):497–503, 2000.

[5] E. Bänsch, F. Haußer, O. Lakkis, B. Li, and A. Voigt. *J. Comput. Phys.*, 2003 (to appear).

[6] E. Bänsch, F. Haußer, and A. Voigt. Technical Report 36, research center caesar, 2003.